Journal of Earth Science, *Vol. 33*, *No. 3*, *p. 552−566*, *June 2022* *ISSN 1674-487X*
Printed in China
https://doi.org/10.1007/s12583-021-1584-y

A Synthesis of Geophysical Data in Southeastern North China Craton: Implications for the Formation of the Arcuate Xuhuai Thrust Belt

Yangfan Deng*[1, 2], Yun Chen[2, 3], Pengfei Li[1, 2], Zhou Zhang[1, 2], José Badal[4]
1. *State Key Laboratory of Isotope Geochemistry*, *Guangzhou Institute of Geochemistry*, *Chinese Academy of Sciences*, *Guangzhou* 510640, *China*
2. *CAS Center for Excellence in Deep Earth Science*, *Guangzhou* 510640, *China*
3. *State Key Laboratory of Lithospheric Evolution*, *Institute of Geology and Geophysics*, *Chinese Academy of Sciences*, *Beijing* 100029, *China*
4. *Physics of the Earth*, *Sciences B*, *University of Zaragoza*, *Pedro Cerbuna* 12, 50009 *Zaragoza*, *Spain*
Yangfan Deng: https://orcid.org/0000-0003-3994-9865

ABSTRACT: The Xuhuai fold thrust belt (XHTB) is a curved structure in the southeastern margin of the North China Craton (NCC) that has attracted great attentions due to its tectonic and petrological characteristics. However, few geophysical studies have focused on the deep structure of this belt. In this study, we carry out a systematic demonstration of the main geophysical features that characterize the XHTB and surrounding areas. The results reveal small negative gravity and magnetic anomalies, thin crust and lithosphere, lower shear velocity and shallower earthquake epicenters relative to other areas of the NCC, collectively indicating a lithospheric-scale rheological anomaly at this belt. The magnetic alignments show a trend similar to that of geological units in southeastern NCC and adjacent areas, although they differ from the SKS-splitting fast polarization directions, except in the Qinling-Dabie orogen where a vertical coherent deformation of the crust and mantle may be involved there. Based on the geophysical data, we propose a detachment-controlled model, which was caused by the different detachment depth/strength, for the formation of XHTB to explain its arcuate shape as well as the magnetic alignments, thus providing new insight into the deep processes of southeastern NCC.
KEY WORDS: gravity and magnetic anomalies, shear wave velocity, seismicity, seismic anisotropy, magnetic alignments, arcuate structure.

0 INTRODUCTION

Global fold-thrust belts commonly show map-view curvatures that are commonly referred to salients, recesses, arcs, oroclines, or syntaxes (Livani et al., 2018; Li et al., 2017; Marshak, 2004; Weil and Sussman, 2004). This characteristic shape can be formed due to different factors, for example, the detachment depth or strength and the detachment slope (Marshak, 2004, 1988). Different models have been proposed to explain the arc-shaped fold belts (Schellart et al., 2007; Marshak, 2004; Macedo and Marshak, 1999), namely: (a) basin-controlled salient; (b) interaction with foreland obstacles; (c) indenter-controlled salient; (d) detachment-controlled salient; (e) interaction with strike-slip faults; (f) salient generated by intersection curves; (g) margin-controlled salient; (h) slab-controlled salient; (i) trench retreat salient (Fig. 1). To understand the origin of the curved geometry, it is vital to unravel the deep structure of the fold thrust belts.

The Xuhuai fold-thrust belt (hereafter XHTB) or Xuhuai orocline is located in the southeastern margin of the North China Craton (NCC) and to the west of the Sulu Orogen (SLO), adjacent to the Tanlu fault (TLF). Structurally, it appears as a convex fold thrust belt (Fig. 2), but there is no significant difference in elevation from nearby regions. Like other curved belts that reflect certain geological evolution, the XHTB is considered one of the key regions to study the continental collision between the NCC and the Yangtze block that started in the Triassic (Shu et al., 2017; Zhang and Dong, 2008). This collision resulted in the Qinling-Dabie-Sulu orogenic belt and HP/UHP metamorphic rocks (Zheng, 2008). The curved XHTB, together with the large active strike-slip fault of Tanlu, the metamorphic HP/UHP orogenic belt (Qinling-Dabie-Sulu Orogen) and the conjunction between the Yangtze Block and the North China Craton, make this area complex and a key region for understanding the continental collision.

Various explanations have been given for the formation of the XHTB: the earliest studies advanced that this belt is a nappe structure due to the over-thrusting of the Yangtze Block

*Corresponding author: Yangfandeng@gig.ac.cn

Manuscript received October 8, 2021.
Manuscript accepted November 18, 2021.

Deng Yangfan, Chen Yun, Li Pengfei, Zhang Zhou, Badal José, 2022. A Synthesis of Geophysical Data in Southeastern North China Craton: Implications for the Formation of the Arcuate Xuhuai Thrust Belt. *Journal of Earth Science*, 33(3): 552–566. https://doi.org/10.1007/s12583-021-1584-y. http://en.earth-science.net

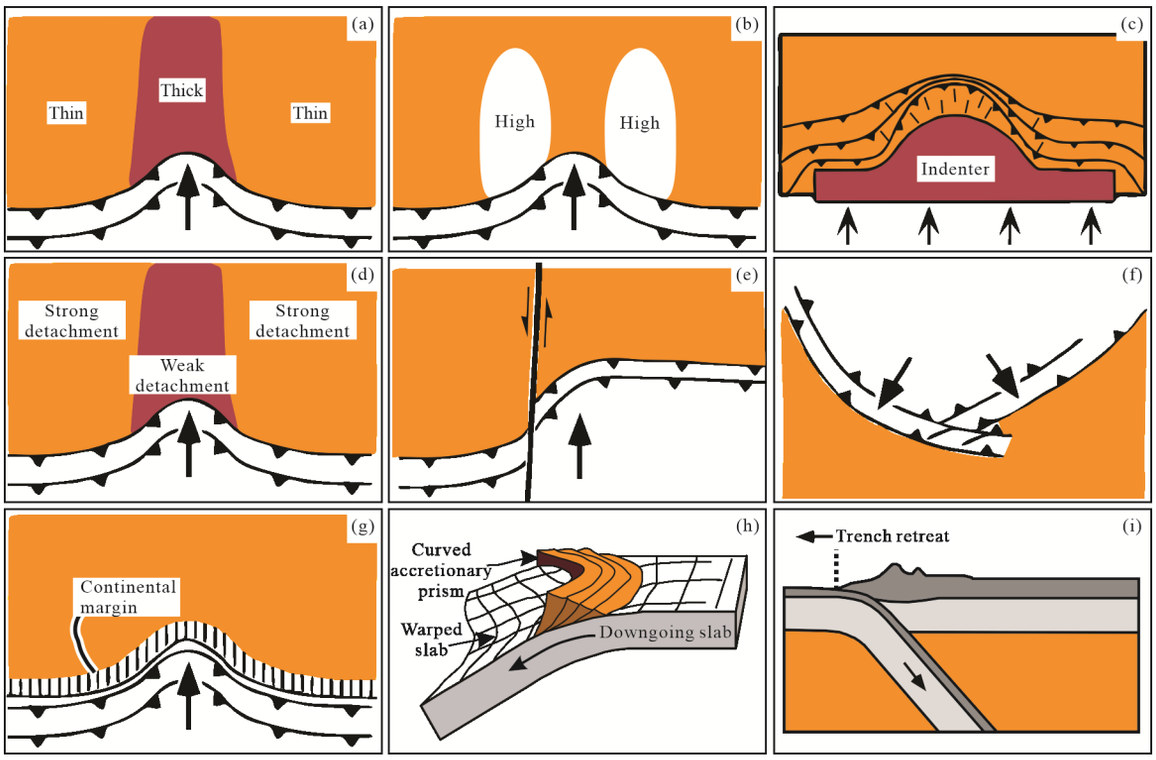

Figure 1. Nine classic models that explain the characteristic arcs in fold belts: (a) basin-controlled salient; (b) interaction with foreland obstacles; (c) indenter-controlled salient; (d) detachment-controlled salient; (e) interaction with strike-slip fault; (f) salient generated by intersection curves; (g) margin-controlled salient; (h) slab-controlled salient; (i) trench retreat salient (modified after Schellart et al., 2007; Marshak, 2004; and Macedo and Marshak, 1999).

on the NCC (Wang et al., 1998; Xu et al., 1987). Based on structural observations, Li (1994) considered that the belt is a detachment structure due to gravity extension, while Zhang and Dong (2008) proposed that it is the result of lateral extrusion of SLO due to the collision. Sun et al. (2010) and Ling et al. (2013), based on geochemical evidence, suggested that the belt may have originated from the ridge subduction along the NCC during the Mesozoic. Zhao et al. (2016) argued that the XHTB is the result of the under-thrusting of the Yangtze Block during the Middle Triassic, and Zhu et al. (2009) proposed that the XHTB is the original northwest corner of the SLO. Another study has proposed that the XHTB was generated by intracontinental underthrusting in the SE margin of the NCC during the Middle Mesozoic, in the framework of the so-called "thin-skin tectonics" (Shu et al., 2017). However, all these models are based on surface structures and/or geochemical studies, but are not constrained by geophysical data.

The geophysical data can shed light on the deep structure and 3D geometry of the Xuhuai fold-thrust belt, which is crucial to complement the observations made on the surface. In this sense, some projects have been conducted in the nearby regions. For example, the SinoProbe program and the National Key R&D Program have provided a large amount of seismic data and valuable results (Chen et al., 2019; Li et al., 2018; Zhang et al., 2015; Xu et al., 2014; Dong et al., 2013; Jiang et al., 2013; Lü et al., 2013). However, purely seismic data alone do not provide sufficient information about the physical state of the lithosphere, since the P- and S-wave velocities are controlled by many factors, such as density, temperature and volatile content of the crust and upper mantle (Mooney and Kaban, 2010). In this study, we present a comprehensive geophysical dataset related to the XHTB and adjacent areas, including gravity and magnetic anomalies, seismic velocity, Moho depth, seismicity and anisotropy. Based on these data, we propose a detachment-controlled model to explain the formation of the arcuate XHTB.

1 GEOLOGICAL SETTING

The collision between the Yangtze Block and the NCC in the Triassic led to the formation of one of the world's largest belts of metamorphic UHP rocks, called the Qinling-Dabie-Sulu Orogen (Meng and Zhang, 1999). The XHTB, located southeast of the NCC (Fig. 2), is known for large-scale coal deposits found among the Late Paleozoic strata near the western edge of the belt (Shu et al., 2017). According to the geological study carried out by Shu et al. (2017), three structural units can be distinguished in the XHTB: (1) The pre-Neoproterozoic crystalline basement in the eastern segment. (2) The nappe unit or thrust-and-fold zone in the central segment, which is composed of carbonate rocks from the Neoproterozoic to the Ordovician and coal-bearing rocks of the Carboniferous–Permian approximately 2 600 m thick. (3) The western frontal zone. Field observations and drill-hole data have demonstrated that the thrusting and folding of the XHTB took place after the deposition of the Early Permian coal-bearing rocks and prior to the deposition of the Early Cretaceous volcano-clastic beds, thus suggesting an Early Mesozoic age (i.e., Triassic to Jurassic) for the deformation (Shu et al., 2017). Jurassic and Cretaceous intrusive rocks associated to periods of 190–188, 160–150, and 135–110 Ma are exposed in the XHTB (Yang et al., 2008; Zhang and

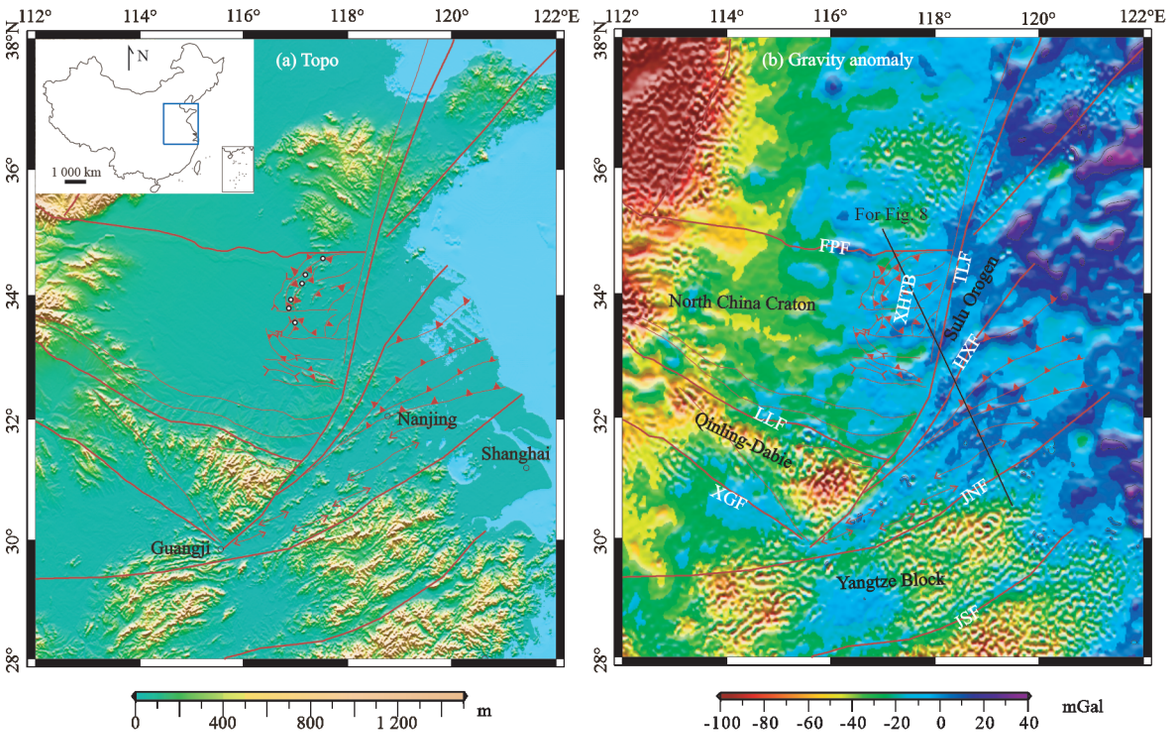

Figure 2. (a) Topography and main geological units in the southeastern North China Craton (NCC). The inset in the top left corner shows the study region in Chinese mainland contoured by a rectangle (modified after GS(2016)1552). The topography comes from the Etopo1 model which can be accessed through the link (https://www.ngdc.noaa.gov/mgg/global/global.html). Intrusive rocks in the Xuhuai fold belt are marked by small white circles. Tectonic units are taken from Zhang and Dong (2008) and Dong et al. (2011). (b) Bouguer gravity anomaly based on the Earth Gravitational Model 2008 (EGM 2008). The black straight line indicates the location of the profile that we will refer later. XHTB. Xuhuai fold-thrust belt; TLF. Tanlu fault; HXF. Huaiyin-Xiangshui fault; JNF. Jiangnan fault; JSF. Jiangshan-Shaoxing fault; FPF. Fengpei fault; LLF. Luonan-Luanchuan fault; XGF. Xiangfan-Guangji fault.

Dong, 2008; Xu et al., 2006), and they did not experience the orocline deformation (Xu et al., 2006).

The TLF (Fig. 2b) has undergone multi-stage structural deformations since the Mesozoic, thus showing distinct properties during different periods, such as left-lateral strike slip in the Early Cretaceous, extensional deformation during the Late Cretaceous and Paleogene, and compression and right-lateral strike slip since the Neogene (Zhu et al., 2004). Other studies suggested a recent right-lateral strike-slip with a minor normal component (Yin, 2010; Zhang et al., 1999). An indentation model was also proposed to explain the evolution of the TLF (Yin and Nie, 1993). The crustal-scale north-to-south segmentation of this major fault has been demonstrated from an integrated geophysical data set (Deng et al., 2013; Zhang and Dong, 2008).

2 GEOPHYSICAL DATA

2.1 Bouguer Gravity Anomaly

Bouguer gravity anomaly reflects the effect of gravity of all masses below the surface that differ from the Earth's reference density (Meurers, 2017). In general, Bouguer gravity adds up all the changes or anomalies in density due to the non-homogeneous structure of the lithosphere as consequence of shallow material deposits, different geological formations and the undulation or dipping of the layers (Zeng, 2005). We have compiled the Bouguer gravity map for the study region (Fig. 2b) from the Earth Gravitational Model 2008 (EGM 2008) reported by Pavlis et al. (2012). This model, based on the GRACE terrestrial gravity anomaly, includes spherical harmonic coefficients up to the order 2159. The standard deviation of the field data is less than 5 mGal.

The negative gravity anomaly is mainly distributed west of the TLF, including the low negative anomaly in the XHTB, while the positive gravity anomaly spans the entire area east of the TLF (Fig. 2b). In addition, this positive gravity anomaly shows some linear trends, which correlates well with the fault zones. For example, the area near and around the TLF is characterized by approximately +10 mGal. The gravity anomaly associated to the Huaiyin-Xiangshui fault reaches +20 mGal. The positive gravity anomaly can originate from magmatic intrusion, as inferred by shear-wave velocity inversion (Bem et al., 2020). Alternatively, the elevation of the Moho discontinuity may be another reasonable explanation, as this feature has been observed in several dense seismic profiles (Liu et al., 2015; Deng et al., 2013; Chen et al., 2006). We will distinguish them in the later section.

2.2 Magnetic Anomalies

Magnetic anomaly is a local variation of the Earth's magnetic field resulting from changes in the magnetism of the rocks that include iron ore with magnetite minerals and mafic igneous or metamorphic rocks with ferromagnesian minerals (Guan, 2005). Magnetic anomalies represent structural and/or compositional differences at depths where the temperature is

below the Curie point. Essentially, the magnetic anomalies are a response to the characteristics of the crust. We have compiled the magnetic anomaly map for the study area (Fig. 3a) from airborne measurements in the southeast of the NCC conducted by the China Aerospace Geophysical Survey and Remote Sensing Centre for Lands and Resources (Xiong et al., 2016).

The distribution of the magnetic anomaly in the Xuhuai region, with a resolution of 2 km, also shows some linear trends. The conjunction zone between the NCC, the Qinling-Dabie Orogen and the Yangtze Block shows a clear negative anomaly, while the TLF exhibits a linear positive anomaly along its strike. In change, the magnetic anomaly in the XHTB is rather variable: it is negative towards the center of the belt, but mostly positive to the north and the south.

The total magnetic anomaly is affected by the inclination of the Earth's magnetic axis. The reduction-to-pole (RTP) transformation (Luis and Miranda, 2008) of total field magnetic anomalies is used to eliminate the asymmetry effect caused by such inclination. The RTP operation causes the anomalies to overlap the sources, and allows magnetic anomalies to be correlated with other types of geophysical anomalies (e.g., gravity) or with geological information, which is an aid to interpretation (Ravat, 2007). The magnetic anomaly map after RTP (Fig. 3b) shows clearer features, compared to the total magnetic anomaly (Fig. 3a). For example, the TLF exhibits a remarkable linear positive anomaly. Ore deposits located in the Yangtze metallogenic belt also appear to be associated with high positive anomalies. We should note that there is a notable linear positive anomaly along 116° E, which may indicate a significant boundary.

2.3 Seismic Velocity Sections

Based on direct surface wave tomography (DSurfTomo) (Fang et al., 2015), Bem et al. (2020) performed 3D crustal shear-wave velocity tomography using 29 temporary broadband seismic stations and 61 permanent seismic stations deployed in southeastern NCC that includes the XHTB. The horizontal resolution is ~50 km and the vertical resolution is ~10 km, as they demonstrated in their paper. Taking advantage of the results of the tomography, in Fig. 4 we show horizontal S-wave velocity slices at depths of 5, 15, 20, and 30 km. In addition, we show two other cuts at mantle depths of 70 and 90 km, obtained by joint inversion of receiver functions and surface wave dispersion (Li et al., 2018). A relatively low velocity zone extends beneath the Subei Basin and, to a lesser extent, below the Hefei Basin, in correspondence with the sedimentary structure of both basins (Fig. 4a). In contrast, the Qinling-Dabie Orogen, XHTB and the Sulu Orogen exhibit high velocity. Low velocity characterizes the Subei Basin at a depth of 15 km (Fig. 4b), indicating that the sedimentary layer affect this depth in this area. Relatively high shear velocity still characterizes the XHTB in the upper crust (15 km), but is absent in the middle crust (20 km), where low velocities are the general feature at this depth (Fig. 4c). The S-velocity pattern at 30 km reveals the Moho depth (Fig. 4d). The high velocity between the Tanlu fault and the Huaiyin-Xiangshui fault reveals a comparatively shallow Moho, while the low velocity in the Qinling-Dabie Orogen and the XHTB reveals a thick crust, which is consistent with the results provided by two-steps surface wave tomography (Meng et al., 2019). At mantle depth, TLF exhibits low velocities (Figs. 4e, 4f).

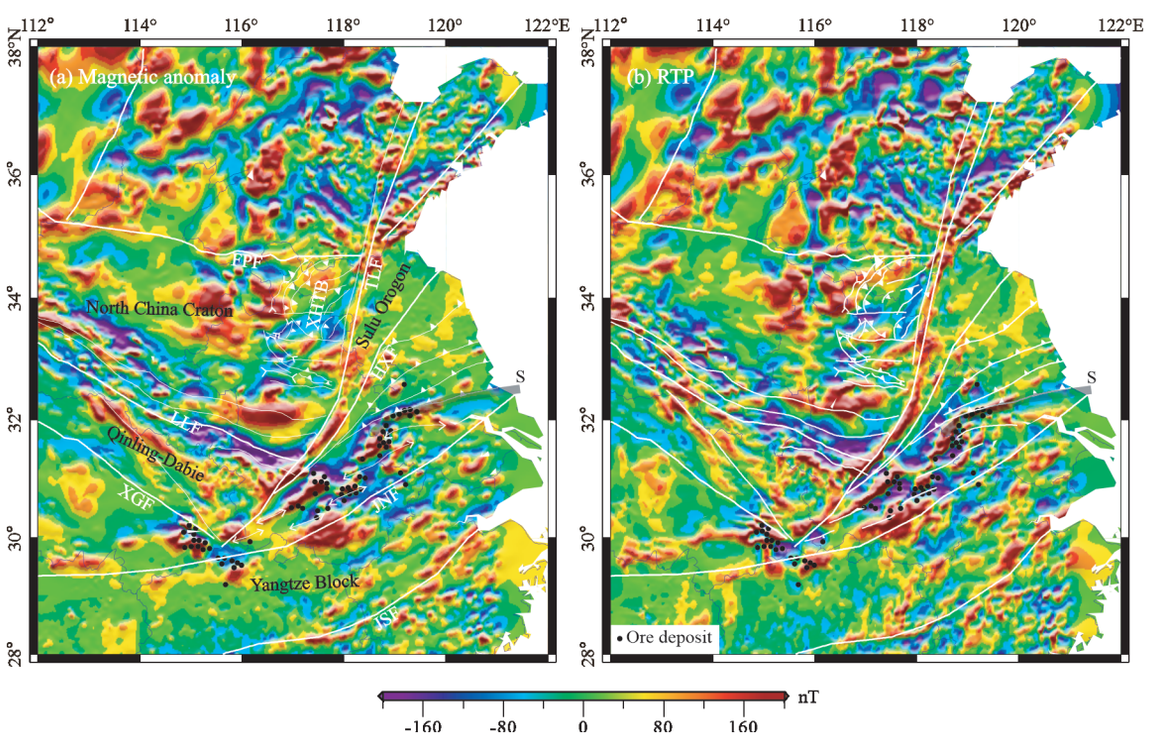

Figure 3. (a) Magnetic anomaly map compiled from airborne measurements in southeastern NCC conducted by the China Aerospace Geophysical Survey and Remote Sensing Centre for Lands and Resources. (b) Magnetic anomaly after reduction-to-pole (RTP). Regions containing ore deposits are indicated by black dots. Geological units and faults are the same as in Fig. 2.

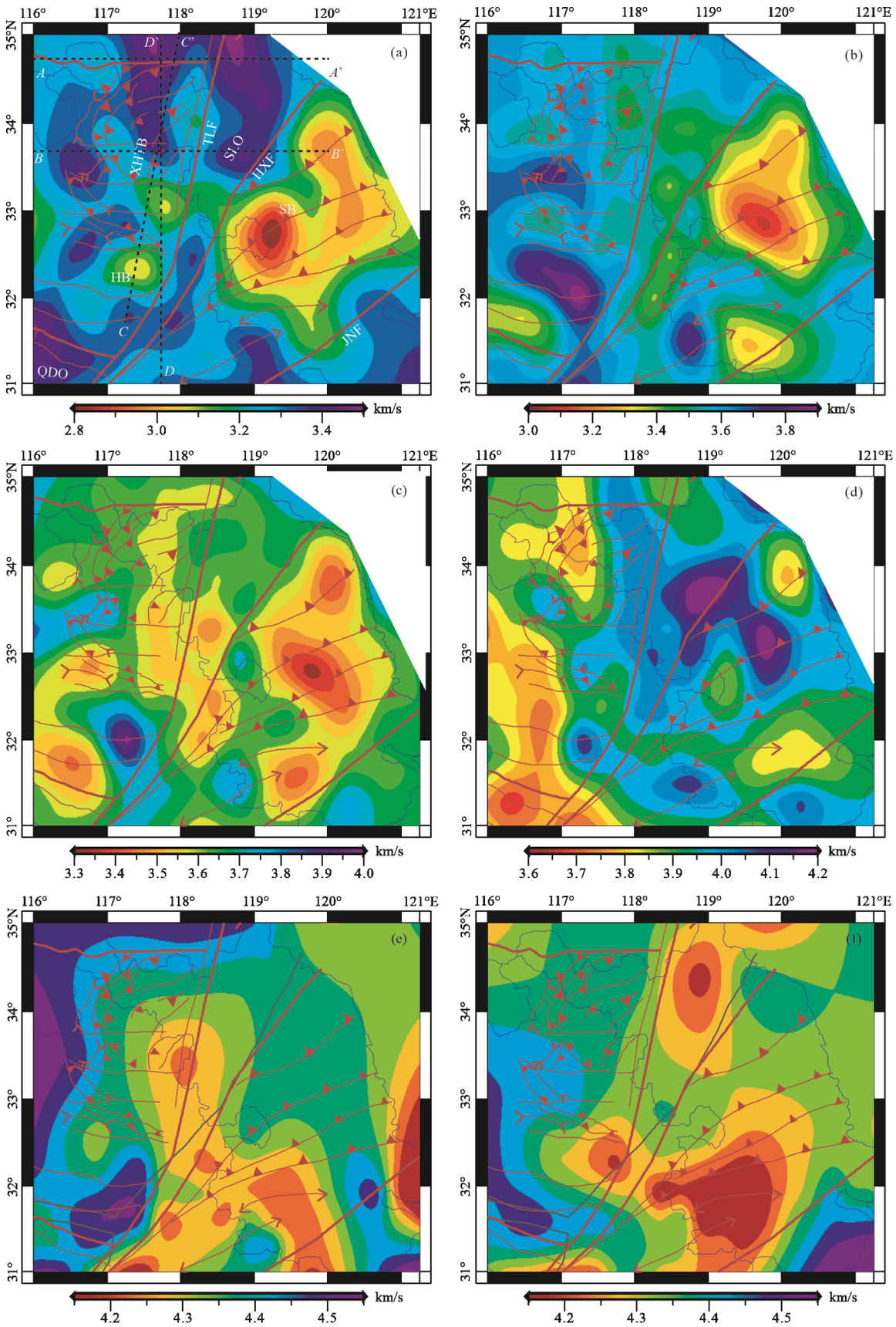

Figure 4. S-wave velocity sections at depths of (a) 5, (b) 15, (c) 20, (d) 30, (e) 70, and (f) 90 km in southeastern NCC. Crustal velocity data are taken from Bem et al. (2020) and mantle velocity data from Li et al. (2018). The dashed lines in (a) indicate the location of four profiles *A-A'*, *B-B'*, *C-C'* and *D-D'* to which we will refer later. QDO. Qinling-Dabie Orogen; HB. Hefei Basin; SLO. Sulu Orogen; SB. Subei Basin. The rest of acronyms are the same as in Fig. 2.

2.4 Moho Depth and Lithosphere-Asthenosphere Boundary

Receiver functions are a good tool to estimate the depth of seismic interfaces, while surface wave dispersion is sensitive to vertical shear-velocity averages. Since these two types of data are complimentary, joint inversion of receiver functions and surface wave dispersion has been widely used to determine the Moho depth. Classical joint inversion usually set the V_p/V_s ratio as a constant, which influences the accuracy of the result. Taking into account this fact, Li et al. (2018) first obtained the V_p/V_s ratio at each station using the *H-k* stacking algorithm (Zhu and Kanamori, 2000), and then determined the Moho depth from the joint inversion of receiver functions and surface wave dispersion data recorded at 191 stations deployed in East-Central China. Figure 5a shows the Moho depth beneath different stations deployed in the study area. The region with the thinnest crust is east of the TLF, which agrees with the high S-wave velocity at 30 km depth independently detected in this region (Fig. 4d), and also compatible with recent studies (Hong et al., 2021; Li et al., 2021). A thicker crust appears west of the TLF and especially east of the Qinling-Dabie Orogen. Unfortunately, the stations installed in the XHTB are not enough to give an overall estimate of the Moho depth.

Chen (2010) obtained the thickness of the lithosphere in most of the areas of the NCC, but without sufficient coverage in the XHTB. Based on the joint constraint of topography, gravity, seismic velocity and temperature, Deng and Levandowski (2018) obtained the lithospheric thickness under the condition of flexural isostasy beneath East China. Figure 5b shows the topography of the bottom of the lithosphere in the study region, that is, the lithosphere-asthenosphere boundary (LAB). The Qinling-Dabie Orogen exhibits a thick lithosphere, unlike the XHTB that shows a thin lithosphere. It should be noted that this flexural lithospheric thickness is different from the thickness determined only from seismic data; a detailed comparison can be seen in Deng and Levandowski (2018).

2.5 Earthquake Distribution

The spatial distribution of earthquakes indicates the stress state of a certain region. In particular, the focal depth reflects the brittle-ductile transition of the rocks. In Fig. 6 we show the earthquake distribution map in southeastern NCC during the period 2008–2019, which was archived from the China Earthquake Networks Center database. The colors make it possible to distinguish different focal depths. Lacking new epicentral relocations, the managed catalog is sufficient to show different clusters of earthquakes related to some geological units. Strong seismicity is observed in the northern segment of the TLF, where the big *M*8.5 Tancheng earthquake occurred in July 25, 1668. However, there is a significantly lower number of earthquakes in the XHTB compared to the nearby regions (Fig. 6). Almost all earthquakes occurred west of the TLF have focal depths equal to or less than 10 km. In contrast, many of the earthquakes with epicenter in the region between the Huaiyin-Xiangshui fault and the Jiangnan fault have a focal depth of approximately 20 km and even greater.

3 GEOLOGICAL CONTACTS CONSTRAINED BY NEW GRAVITY AND MAGNETIC MAPS

As a major strike-slip fault in eastern China, TLF exhibits a positive gravity anomaly (Fig. 2b) along with a positive magnetic anomaly (Fig. 3b). By contrast, the Luonan-Luanchuan fault (LLF in Fig. 2b) clearly shows a negative magnetic anomaly (Fig. 3b). Shallow geological variations generate high-frequency gravity and magnetic anomalies, while changes in the magnetic and gravity properties at deeper depth generate low-frequency anomalies (Guan, 2005). To investigate the deep origin of such geological contacts, we apply the new data processing method in the spatial domain proposed by Guo and Tao (2020). This algorithm allows the calculation of potential field data either upward or downward from the surface to a plane. Following this method, in Fig. 7 we show the gravity anomaly maps obtained by upward continuation from the surface to 10

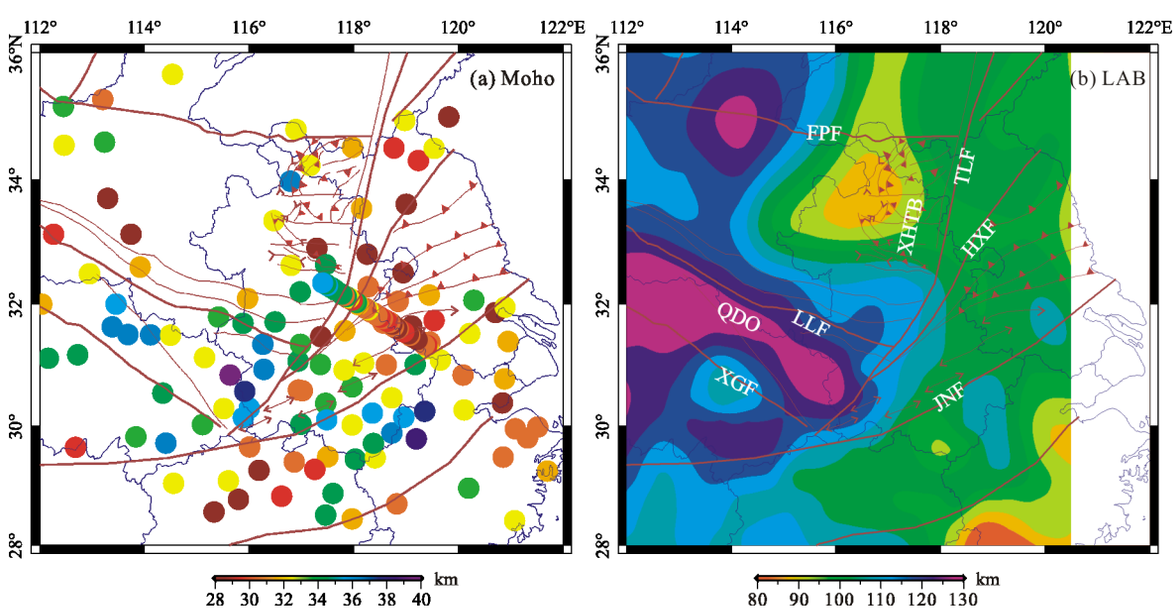

Figure 5. (a) Moho depth at different locations (colored circles) after Li et al. (2018). (b) Depth of the isostatic flexural limit corresponding to the lithosphere-asthenosphere boundary (LAB) after Deng and Levandowski (2018). Geological units and faults are the same as in Fig. 2.

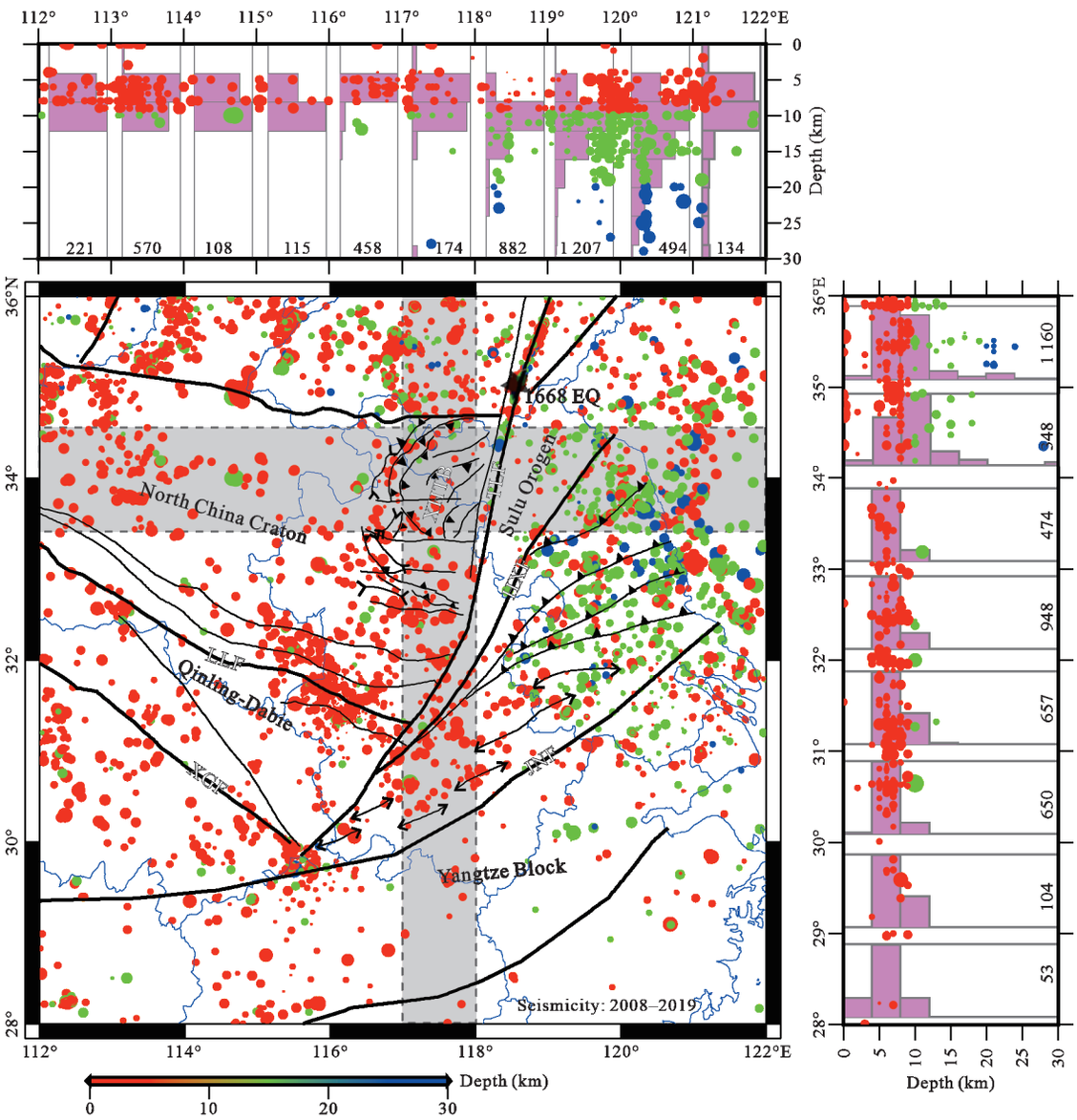

Figure 6. Central panel: spatial distribution of earthquake epicenters (circles) in southeastern NCC during the period 2008–2019. Color indicates focal depth (see depth scale in km). Top and right panels: hypocenters and released energy (bar histograms) along geographic longitude and latitude. The number included within each column indicates the energy released in the corresponding region. Black star (top in central plot) indicates the epicenter of the 1668 Tancheng Earthquake. Data are provided by the China Earthquake Networks Center (CENC). Geological units and faults are the same as in Fig. 2.

and 30 km (Figs. 7a and 7b), and also the corresponding magnetic anomaly maps obtained by the same procedure (Figs. 7c and 7d). As shown in the two gravity maps, TLF appears contoured by a positive anomaly, especially on its eastern side, leading us to believe that this boundary is a major fault penetrating deeply. The XHTB shows a low negative anomaly compared to other regions further west of the TLF, which indicates a variation in the structure and composition of the crust. Likewise, a well-defined negative gravity anomaly with a deep origin is observed in the Qinling-Dabie Orogen. In view of the two magnetic anomaly maps, both the Tanlu fault, which shows positive values, and the Luonan-Luanchuan fault, characterized by negative values, appear to be major faults on a lithospheric scale. Now more clearly, the positive magnetic anomaly along 116°E may reflect another tectonic boundary.

In order to investigate more about the origin of the linear positive gravity anomaly detected in southeastern NCC, in Fig. 8a we show the Bouguer gravity curve along a reference profile (see Fig. 2b), as well the curves obtained by upward continuation (Guo and Tao, 2020) at 10 and 30 km. The highest gravity values around +10–15 mGal correspond to the central segment of the profile, where the Huaiyin-Xiangshui fault and the Tanlu fault are intersected by the profile, and the half wavelength of these anomalies is ~20 km. These anomalies decrease notably with reference to the plane at 10 km and vanish at 30 km, indicating that the linear positive anomaly has a shallow origin.

To better discern the origin of the observed gravity anomaly, we simulate the gravity field under various assumptions, that is, modeling some density anomalies embedded in the crust at different depths, as shown in Fig. 8c. In this illustration, the anomalous density blocks reflect the following struc-

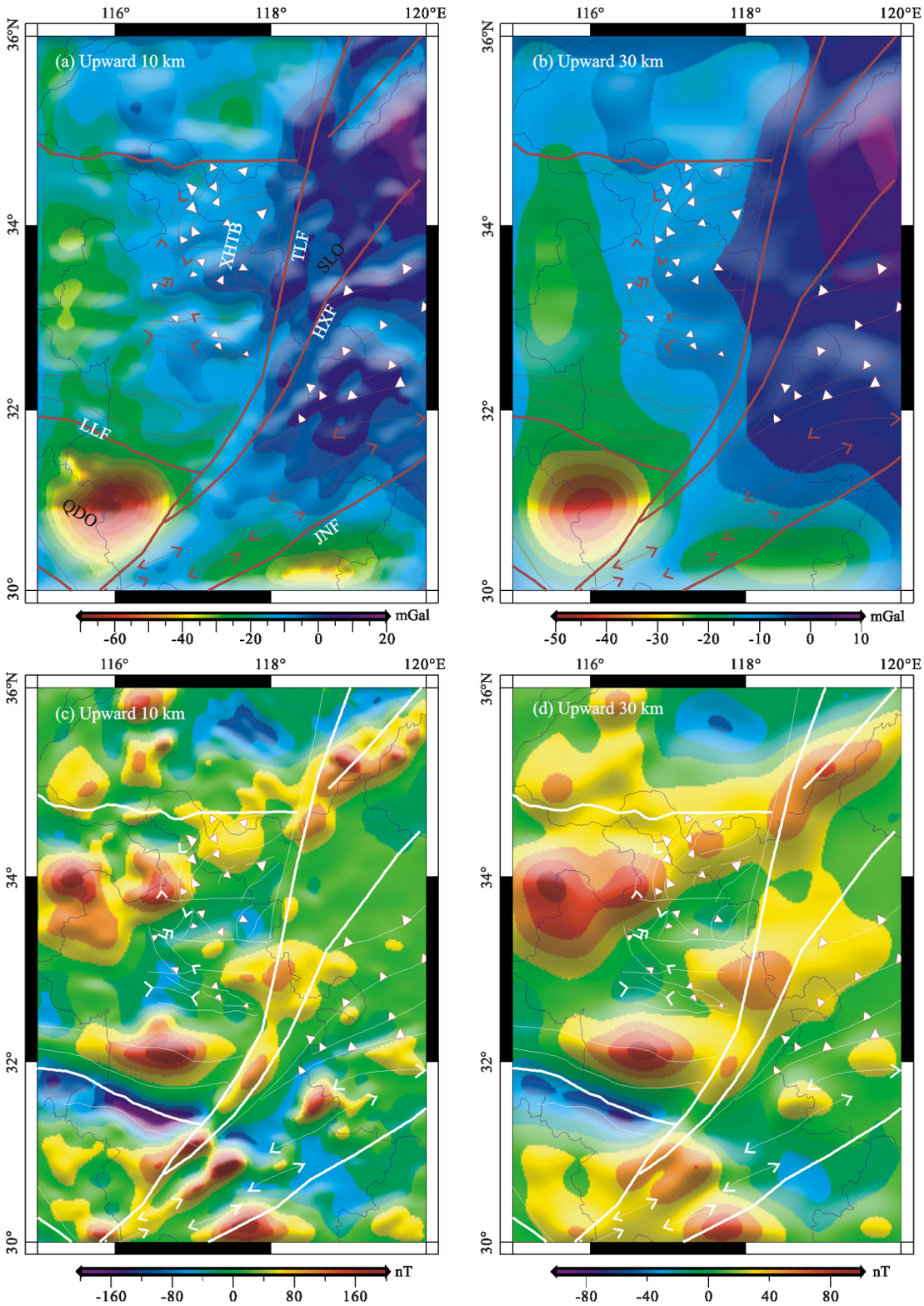

Figure 7. (a), (b) Gravity anomaly maps after upward continuation (Guo and Tao, 2020) at 10 and 30 km. (c), (d) Magnetic anomaly maps obtained by the same procedure. Geological units and faults are the same as in Fig. 2.

tures: A, shallow structure; B, upper crust; C, middle crust; D, lower crust; E, middle-to-lower crust. Each of these 5 × 5 km^2-sized boxes represent a magmatic intrusion or strata with a density contrast of 0.2 g/cm^3 (Deng et al., 2016). The block D represents an elevation of the Moho, while the 5 × 15 km^2-sized block E, also with density contrast of 0.2 g/cm^3, located at 15–30 km depth, could represent intrusive rocks embedded in the middle-to-lower crust. Figure 8b shows the synthetic gravity anomaly curve. For comparison, we show the observed Bouguer gravity anomaly near the Chaohu-Gaoyou, Huaiyin-Xiangshui

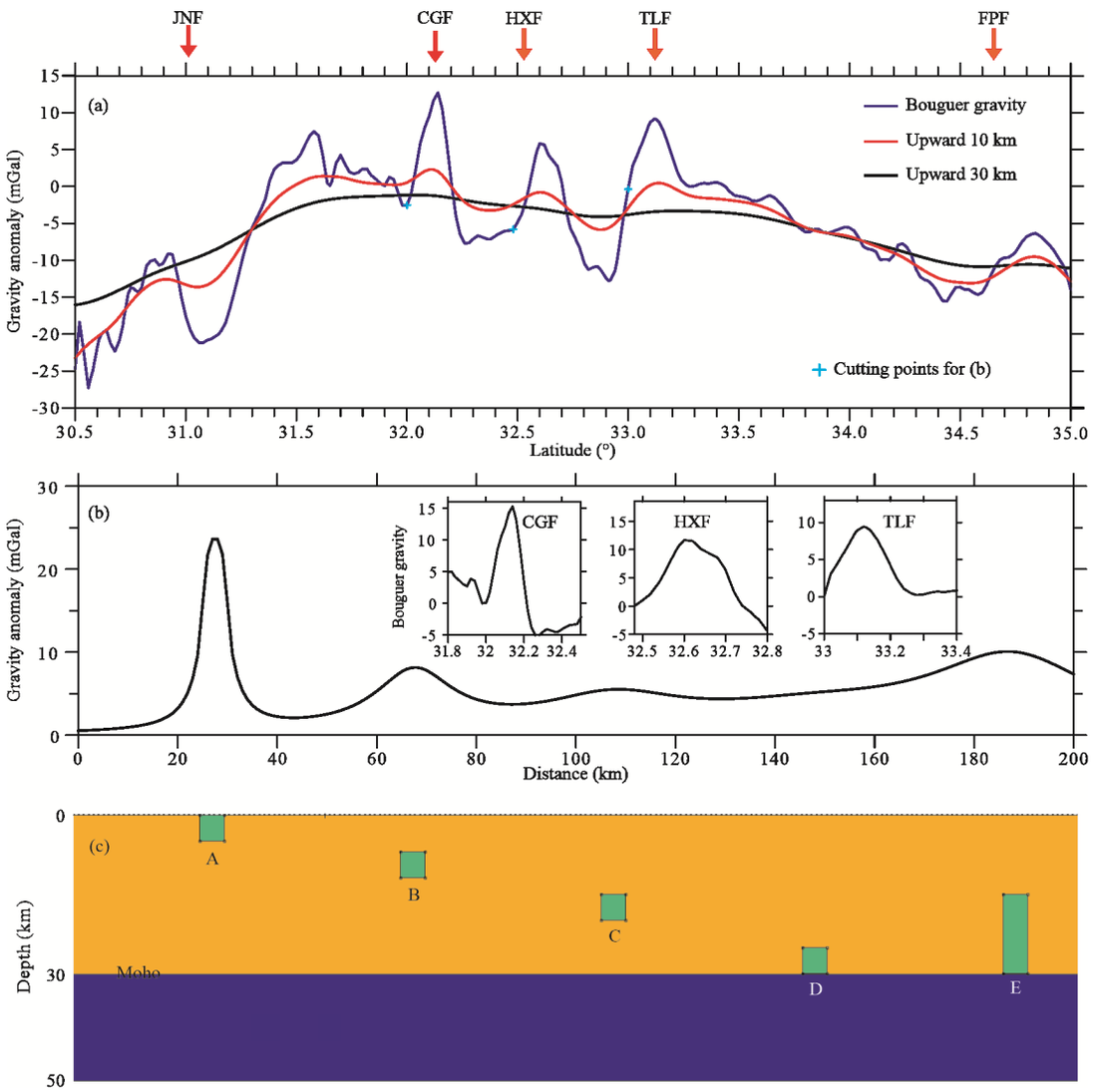

Figure 8. (a) Gravity anomaly curves along the NW-SE reference profile (see Fig. 2b), including Bouguer gravity (blue line) and gravity anomalies obtained by upward continuation (Guo and Tao, 2020) at 10 (red line) and 30 km (black line). Faults intersected by the profile (from south to north): JNF. Jiangnan fault; CGF. Chaohu-Gaoyou fault; HXF. Huaiyin-Xiangshui fault; TLF. Tanlu fault; FPF. Fengpei fault. (b) Synthetic gravity anomaly curve obtained after modeling different density anomalies depicted below. For comparison, we show the observed Bouguer gravity anomaly near the Chaohu-Gaoyou, Huaiyin-Xiangshui and Tanlu faults (CGF, HXF and TLF insets included in this panel). (c) Blocks of size 5 × 5 km^2 and density of 0.2 g/cm^3 embedded at different depths in the crust: A. near-surface density anomaly; B. anomaly at 9.5 km depth (upper crust); C. anomaly at 17.5 km depth (middle crust); D. anomaly at 27.5 km depth (lower crust); E. 5 × 15 km^2-sized block at 15–30 km depth (middle-to-lower crust). The block labeled D represents an elevation of the Moho, while the block labeled E depicts intrusive rocks embedded in the middle-to-lower crust.

and Tanlu faults (CGF, HXF and TLF insets included in this panel). Obviously, blocks like C, D or E cannot generate the observed Bouguer anomaly, since the amplitude of the produced anomaly is smaller and the wavelength is wider. However, an A-type density contrast or even B-type could generate a gravity anomaly of ~20 mGal and to a lesser extent of ~10 mGal, with a half wavelength of 20 km. Therefore, we conclude that a density anomaly at a relatively shallow depth (in the upper crust), such as a dipping/overlapping formation or intrusive mafic/metamorphic rocks, appears to be the trigger factor for the linear trend gravity anomaly in southeastern NCC. The synthetic gravity curve (Fig. 8b) makes it possible to rule out the Moho uplift as the cause of the gravity variation because it cannot generate such a short wavelength anomaly. Recent studies (Xu et al., 2021; Li et al., 2020; Gu et al., 2019; Luo et al., 2019) show a high velocity in the shallow part beneath TLF that is consistent with our interpretation.

4 DEFORMATION CONSTRAINED BY SEISMIC ANISOTROPY AND MAGNETIC ALIGNMENTS

Seismic anisotropy is a useful tool to estimate deformation of the crust and upper mantle (Hu et al., 2018; Chen et al., 2015; Wu et al., 2015). However, the depth of the anisotropy deduced from SKS-splitting measurements remains a problem of some difficulty. Pms-splitting measurements have been used to directly constrain the anisotropy and deformation of the crust and to largely explain the deformation mechanism of the crust (Chen et al., 2013).

Regarding the deformation of the upper crust, Bokelmann and Wüstefeld (2009), based on quantitative magmatic information, used magnetic and seismic anisotropy to compare crustal and mantle fabric, as ferromagnetic minerals in the bulk rock dominate the magnetic properties of the lithosphere. The most magnetic of these minerals is magnetite (Fe_3O_4), which loses its ferromagnetism when the temperature exceeds the Curie point of approximately 580 °C (Bokelmann and Wüstefeld, 2009). Hence, magmatism data can provide the alignment of rocks within the upper-middle crustal fabric.

4.1 SKS-Splitting Based Anisotropy

From the results provided by Huang et al. (2013), Shi et al. (2013), Zhao et al. (2013), Tian and Santosh (2015), Li et al. (2018) and Yang et al. (2019), in Fig. 9a we show SKS-splitting vectors at each station deployed in the explored region. The average splitting parameters show a delay time of ~1.2 s and a fast wave polarization direction to N98ºE. Nevertheless, an E-W fast polarization direction can be observed in the easternmost continental area. From south to north, there does not appear to be a clear change in the polarization direction in the Yangtze Block and the NCC. Tian and Santosh (2015) considered that the subduction of the Pacific Plate during the Cenozoic provoked the change in the fast polarization direction from WNW-ESE to NW-SE, while the E-W fast polarization direction is characteristic of the "fossilized" deformed lithosphere beneath eastern China. More recently, Li et al. (2018) proposed that the westward subduction of the Philippine Plate and the far-field effects of the collision between the Indian and Eurasia plates are the cause of the E-W fast polarization direction during the Cenozoic.

4.2 Magnetic Alignments

In order to compare the results of seismic anisotropy with those derived from the magnetism of the crustal fabric, we apply the Radon transform to calculate the magnetic alignments at certain points, following the method applied by Bokelmann and Wüstefeld (2009) and Wüstefeld et al. (2010). This transform can be used to detect individual alignments on a map, or to characterize preferential orientations by summing all offsets in an appropriate way (Wüstefeld et al., 2010). During the calculation process, we choose a radius of 80 km because it provides a good resolution (Wüstefeld et al., 2010). Figure 9b shows the magnetic alignments in southeast NCC, which look as a V-shaped pattern with the corner east of the Dabie Orogen. In general, the alignment of magnetic anomalies in the Yangtze Block is approximately E-W and NE-SW, which is consistent with the observed trend of the tectonic units and similar, for example, to what happens with the geological boundaries in southern Mongolia (Guy et al., 2014). In the XHTB, the magnetic alignments accommodate the convex shape of the belt, but they turn to NE-SW near the TLF. West and south of the XHTB, the magnetic alignments are almost E-W.

The magnetic alignments in the Qinling-Dabie Orogen have a clear NW-SE orientation, which is consistent with the orogen trend and with fast polarization directions (Fig. 9a). Many SKS- and Pms-splitting studies conducted west of Qinling-Dabie prove that mantle and crust have a similar trend to deformation, except for some local faults (Hu et al., 2020; Liu et al., 2020; Guo et al., 2019; Xu et al., 2018; Chang et al., 2017; Liu et al., 2017; Kong et al., 2016; Wang et al., 2016; Yu and Chen, 2016). The consistency between magnetic alignments and the results provided by shear wave splitting may indicate vertical coherent deformation of the crust and mantle due to the collision orogen. The results deduced with two other trial radii, 50 and 100 km, are compatible with those of 80 km (Fig. S1).

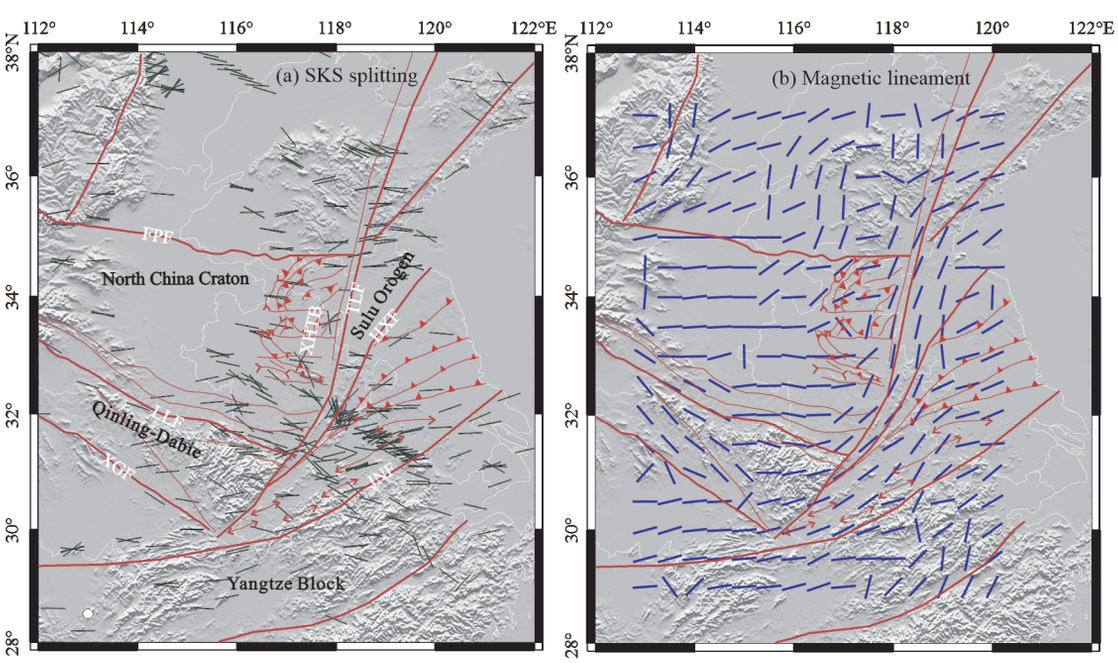

Figure 9. (a) SKS-splitting-based fast polarization directions in the North China Craton (data taken from Yang et al., 2019; Li et al., 2018; Tian and Santosh, 2015; Huang et al., 2013; Shi et al., 2013; Zhao et al., 2013). (b) Magnetic alignments (after reduction-to-pole) in southeastern NCC. In both plots, the red lines represent the main faults and the white lines delineate administrative provinces. Geological units and faults are the same as in Fig. 2.

5 DISCUSSION: DEEP STRUCTURE AND FORMATION OF THE XHTB

To illuminate the deep structure of the XHTB, in Fig. 10 we show four S-wave velocity sections along four profiles, three of which cross the belt (Fig. 4a), in addition to seismicity and topography. According to the *B-B'* profile (Fig. 10b), the Subei Basin shows the lowest velocity in the upper crust compared to the XHTB and the NCC, and the earthquakes occur at deeper depths. The *C-C'* and *D-D'* profiles (Figs. 10c–10d) reveal the existence of a thick crustal low velocity layer beneath XHTB. The bottom of this structure depicts the lower boundary of a detachment layer, along which the region has various depths similar to the fold thrust belt in the Appalachian Orogen (Macedo and Marshak, 1999; Gray and Stamatakos, 1997). On the other hand, the S-wave velocity in the mantle (lower panels in Figs. 10c–10d) and recent Pn-wave tomography model (Yin et al., 2019) show low values in XHTB. This indicates a lithospheric-scale anomaly below XHTB, in which the mantle upwelling changed the crustal rheology. Compared to nearby areas, the few and relatively shallow earthquakes also confirm the weak strength of the XHTB.

Back to the models reviewed in Fig. 1, the margin-controlled salient and the interaction with strike-slip faults do not have this kind of curved shape like the XHTB (Macedo and Marshak, 1999), while the trench or slab controlled salient usually form larger curved fold belts (Li et al., 2017; Schellart et al., 2007). Recent physical modeling supports that a detachment layer plays a key role for the XHTB (Li, 2019; Chen, 2016). However, it is possible to eliminate the basin-controlled orocline when the bottom of the detachment has a depth (e.g., 20 km) that is much deeper than that of a sedimental basin. Furthermore, a detachment-controlled orocline causes the trend lines to converge at the endpoints, not at the indenter-controlled vertex (Macedo and Marshak, 1999). This is consistent with the Xuhuai arc-shaped fold-thrust belt, whose trend lines converge at the endpoints. Moreover, the indenter should have a high velocity, not a low velocity along the strike, as observed in Fig. 10. In addition, we did not find any geological report of the basement uplift to support the obstacle-controlled feature as in the Dabashan orocline (Luo et al., 2020; Wang et

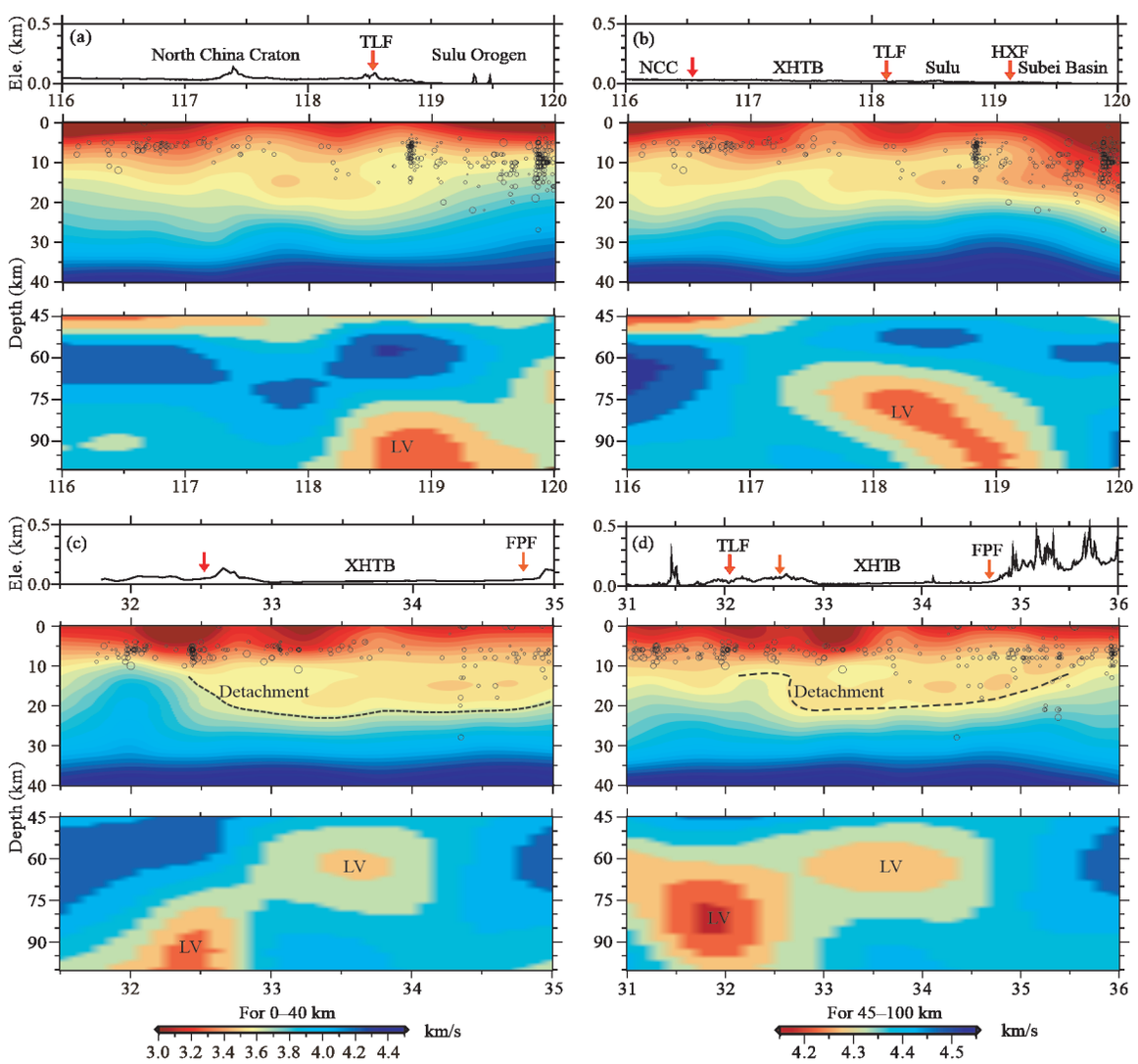

Figure 10. S-wave velocity sections along four reference profiles, namely: (a) *A-A'*, (b) *B-B'*, (c) *C-C'*, (d) *D-D'* (see Fig. 4a). The dashed lines roughly outline the lower boundary of the detachment. Small circles represent earthquake hypocenters. LV means shear velocity. We have added topographic relief and some tectonic references on top of each velocity section. Geological units and faults are the same as in Fig. 2.

al., 2019; Shi et al., 2012), although they may show a similar velocity pattern. Therefore, we suggest the XHTB is a detachment-controlled orocline due to different strengths.

Figure 11 shows a schematic diagram for the possible formation of XHTB. The hot and low velocity mantle material penetrated into XHTB and changed the rheology of the overlying crust, resulting in a thin crust and lithosphere. The orocline was formed in a compressive regime due to the different detachment depth/strength along the strike. As for the reason for the rheological feature of the crust and upper mantle, we can point out various triggers, such as deep subduction of the Yangtze Block below the NCC in Triassic (Shu et al., 2017; Zhao et al., 2016), ridge subduction (Ling et al., 2013, 2009), or western Pacific subduction in Late Mesozoic (Sun et al., 2019). However, we cannot give a concrete answer due to the uncertainty of the chronology, even though Sr-O isotopic studies on apatite suggest that the main dynamic mechanism of diagenesis and mineralization in the Xuhuai area is the result of the subduction of the Pacific Plate (Zhang et al., 2020; Sun et al., 2019, 2007).

The magnetic alignments in the crustal fabric are consistent with the trend of geological units. The effects of the curved geometry as well as the drag induced by the Tanlu strike-slip fault are the cause of the deformation of the magnetic alignments. The SKS-splitting fast directions can be interpreted as the physical response to the westward subduction and retreat of the Pacific Plate, as noted in previous studies (Yang et al., 2019; Li et al., 2018; Tian and Santosh, 2015). In comparison with overthrusting (Wang et al., 1998; Xu et al., 1987), underthrusting (Shu et al., 2017) or extrusion models (Zhang and Dong, 2008), our model is based on the knowledge of the crust-mantle structure supported by geophysical data.

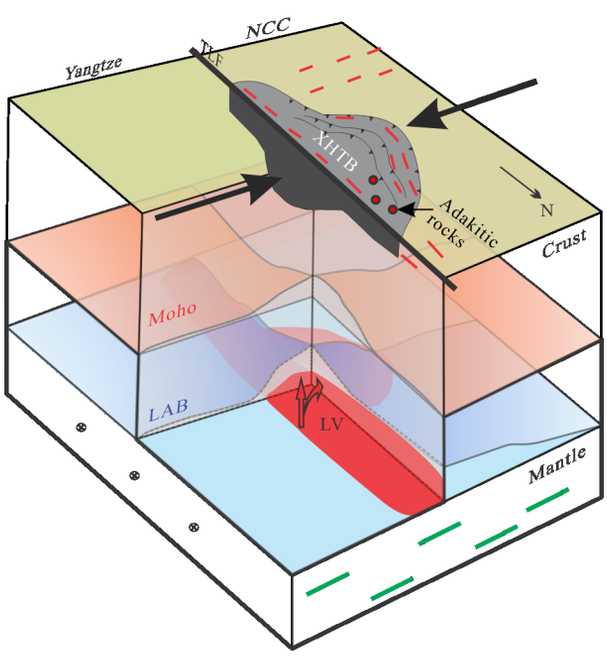

Figure 11. A schematic diagram for the formation of XHTB. The hot and low velocity layer in the mantle changed the rheology of the overlying crust. The orocline was formed in a compressive regime due to the different detachment depth/strength along the strike. Thick arrows represent directions of compressive stress. Red arrows indicate the possible mantle upwelling. Magnetic alignments in the crustal fabric (red dashes) are consistent with the trend of geological units. SKS-splitting fast directions (green dashes and crosses) accommodate to the westward subduction of the Pacific Plate. Adakitic rocks are marked with red circles. The length of the axis is not scaled.

6 CONCLUSIONS

The geophysical information acquired through various datasets, including gravity, magnetic anomalies, shear wave velocity, Moho depth, seismicity and anisotropy, has allowed us to obtain the physical signature related to the geological evolution of the XHTB and nearby regions. The magnetic alignments are consistent with the trend of geological units, with a V-shaped configuration at the corner to the east of the Dabie Orogen. The similarity between the magnetic alignments and the SKS/Pms splitting directions in Qinling-Dabie suggest a coherent deformation in the crust and mantle. New gravity and magnetic anomaly maps obtained by upward continuation confirm that both the TLF and the Luonan-Luanchuan fault are major faults on a lithospheric scale. Density anomalies in the upper crust may be the trigger for the linear positive gravity anomaly in southeastern NCC. The XHTB shows a low negative gravity anomaly, low velocity, thin crust and lithosphere compared to other regions in the west of TLF. A detachment-controlled model for the formation of XHTB is proposed, but the deep process that causes the lithospheric-scale anomaly needs further investigation.

ACKNOWLEDGMENTS

We are very grateful to the China Aerospace Geophysical Survey and Remote Sensing Centre for Lands and Resources for providing the airborne magnetic data. We thank Aaron Price for providing the FastGrav software for gravity modeling, and Prof. Huajian Yao for providing the seismic velocity model. The earthquake catalog has been compiled by the China Earthquake Networks Center. We also benefit from the discussion with Prof. An Yin and Dr. Tülay Kaya-Eken for the earlier version. This study was supported by the National Key R&D Program of China (No. 2016YFC0600402), the National Natural Science Foundation of China (Nos. 41874106, 42021002), the Youth Innovation Promotion Association of CAS (No. YIPA2018385) and the project from Guangdong Province (No. 2019QN01H101). Data on magnetic alignments are available through the link: https://figshare.com/articles/dataset/The_magnetic_lineament_in_East_China/12891035. The final publication is available at Springer via https://doi.org/10.1007/s12583-021-1584-y.

Electronic Supplementary Material: Supplementary material (Fig. S1) is available in the online version of this article at https://doi.org/10.1007/s12583-021-1584-y.

REFERENCES CITED

Bem, T. S., Yao, H. J., Luo, S., et al., 2020. High-Resolution 3-D Crustal Shear-Wave Velocity Model Reveals Structural and Seismicity Segmentation of the Central-Southern Tanlu Fault Zone, Eastern China. *Tectonophysics*, 778: 228372. https://doi.org/10.1016/j.tecto.2020.228372

Bokelmann, G. H. R., Wüstefeld, A., 2009. Comparing Crustal and Mantle Fabric from the North American Craton Using Magnetics and Seismic

Anisotropy. *Earth and Planetary Science Letters*, 277(3/4): 355–364. https://doi.org/10.1016/j.epsl.2008.10.032

Chang, L. J., Ding, Z. F., Wang, C. Y., et al., 2017. Vertical Coherence of Deformation in Lithosphere in the NE Margin of the Tibetan Plateau Using GPS and Shear-Wave Splitting Data. *Tectonophysics*, 699: 93–101. https://doi.org/10.1016/j.tecto.2017.01.025

Chen, B., 2016. Research of Structural Characteristics and Deformation Mechanism in the Xuhuai Region: [Dissertation]. Hefei University of Technology, Hefei (in Chinese with English Abstract)

Chen, L., 2010. Concordant Structural Variations from the Surface to the Base of the Upper Mantle in the North China Craton and Its Tectonic Implications. *Lithos*, 120(1/2): 96–115. https://doi. org/10.1016/j. lithos. 2009.12.007

Chen, L., Zheng, T. Y., Xu, W. W., 2006. A Thinned Lithospheric Image of the Tanlu Fault Zone, Eastern China: Constructed from Wave Equation Based Receiver Function Migration. *Journal of Geophysical Research*: *Solid Earth*, 111(B9): B09312. https://doi.org/10.1029/2005jb003974

Chen, Y., Cui, T., Ding, W. W., et al., 2019. New Progress on the Onshore-Offshore Seismic Survey in East China Continental Margin. *Solid Earth Sciences*, 4(3): 85–91. https://doi.org/10.1016/j.sesci.2019.05.001

Chen, Y., Li, W., Yuan, X. H., et al., 2015. Tearing of the Indian Lithospheric Slab beneath Southern Tibet Revealed by SKS-Wave Splitting Measurements. *Earth and Planetary Science Letters*, 413: 13–24. https://doi.org/10.1016/j.epsl.2014.12.041

Chen, Y., Zhang, Z. J., Sun, C. Q., et al., 2013. Crustal Anisotropy from Moho Converted P_s Wave Splitting Analysis and Geodynamic Implications beneath the Eastern Margin of Tibet and Surrounding Regions. *Gondwana Research*, 24(3/4): 946–957. https://doi. org/10.1016/j. gr. 2012.04.003

Deng, Y. F., Chen, Y., Wang, P., et al., 2016. Magmatic Underplating beneath the Emeishan Large Igneous Province (South China) Revealed by the COMGRA-ELIP Experiment. *Tectonophysics*, 672/673: 16–23. https://doi.org/10.1016/j.tecto.2016.01.039

Deng, Y. F., Fan, W. M., Zhang, Z. J., et al., 2013. Geophysical Evidence on Segmentation of the Tancheng-Lujiang Fault and Its Implications on the Lithosphere Evolution in East China. *Journal of Asian Earth Sciences*, 78: 263–276. https://doi.org/10.1016/j.jseaes.2012.11.006

Deng, Y. F., Levandowski, W., 2018. Lithospheric Alteration, Intraplate Crustal Deformation, and Topography in Eastern China. *Tectonics*, 37(11): 4120–4134. https://doi.org/10.1029/2018tc005079

Dong, Y. P., Zhang, G. W., Neubauer, F., et al., 2011. Tectonic Evolution of the Qinling Orogen, China: Review and Synthesis. *Journal of Asian Earth Sciences*, 41(3): 213–237. https://doi.org/10.1016/j.jseaes.2011.03.002

Dong, S. W., Li, T. D., Lü, Q. T., et al., 2013. Progress in Deep Lithospheric Exploration of the Continental China: A Review of the SinoProbe. *Tectonophysics*, 606: 1–13. https://doi.org/10.1016/j.tecto.2013.05.038

Fang, H. J., Yao, H. J., Zhang, H. J., et al., 2015. Direct Inversion of Surface Wave Dispersion for Three-Dimensional Shallow Crustal Structure Based on Ray Tracing: Methodology and Application. *Geophysical Journal International*, 201(3): 1251–1263. https://doi.org/10.1093/gji/ggv080

Gray, M. B., Stamatakos, J., 1997. New Model for Evolution of Fold and Thrust Belt Curvature Based on Integrated Structural and Paleomagnetic Results from the Pennsylvania Salient. *Geology*, 25(12): 1067–1070. https://doi.org/10.1130/0091-7613(1997)025<1067:nmfeof>2.3.co;2

Gu, N., Wang, K. D., Gao, J., et al., 2019. Shallow Crustal Structure of the Tanlu Fault Zone near Chao Lake in Eastern China by Direct Surface Wave Tomography from Local Dense Array Ambient Noise Analysis. *Pure and Applied Geophysics*, 176(3): 1193–1206. https://doi. org/10.1007/s00024-018-2041-4

Guan, Z. N., 2005. Geomagnetic Field and Magnetic Exploration. Geological Publishing House, Beijing (in Chinese)

Guo, G. H., Wu, C. L., Tang, G. B., et al., 2019. Seismic Anisotropy of the Northeastern Margin of the Tibetan Plateau Derived from Analysis of SKS and Pms Seismic Phases. *Chinese Journal of Geophysics*, 62(5): 1650–1662 https://doi. org/10.6038/cjg2019n0093 (in Chinese with English Abstract)

Guo, Z. K., Tao, C. H., 2020. Potential Field Continuation in Spatial Domain: A New Kernel Function and Its Numerical Scheme. *Computers & Geosciences*, 136: 104405. https://doi. org/10.1016/j. cageo.2020.104405

Guy, A., Schulmann, K., Munschy, M., et al., 2014. Geophysical Constraints for Terrane Boundaries in Southern Mongolia. *Journal of Geophysical Research*: *Solid Earth*, 119(10): 7966–7991. https://doi. org/10.1002/2014jb011026

Hong, D. Q., Huang, X. L., Yang, Y., et al., 2021. Lateral Variation in Moho Depth around the Southern Tanlu Fault Zone and Its Adjacent Area. *Earthquake Science*, 34(1): 77–87. https://doi. org/10.29382/eqs-2020-0063

Hu, J. F., Badal, J., Yang, H. Y., et al., 2018. Comprehensive Crustal Structure and Seismological Evidence for Lower Crustal Flow in the Southeastern Margin of Tibet Revealed by Receiver Functions. *Gondwana Research*, 55: 42–59. https://doi.org/10.1016/j.gr.2017.11.007

Hu, N., Li, Y. H., Xu, L. X., 2020. Crustal Seismic Anisotropy of the Northeastern Tibetan Plateau and the Adjacent Areas from Shear-Wave Splitting Measurements. *Geophysical Journal International*, 220(3): 1491–1503. https://doi.org/10.1093/gji/ggz489

Huang, H., Xu, M. J., Wang, L. S., et al., 2013. Distinct Lateral Variations of Upper Mantle Anisotropy beneath Eastern China Revealed by Shear-Wave Splitting. *Geochemistry*, *Geophysics*, *Geosystems*, 14(6): 1842–1855. https://doi.org/10.1002/ggge.20126

Jiang, G. M., Zhang, G. B., Lü, Q. T., et al., 2013. 3-D Velocity Model beneath the Middle-Lower Yangtze River and Its Implication to the Deep Geodynamics. *Tectonophysics*, 606: 36–47. https://doi. org/10.1016/j. tecto.2013.03.026

Kong, F. S., Wu, J., Liu, K. H., et al., 2016. Crustal Anisotropy and Ductile Flow beneath the Eastern Tibetan Plateau and Adjacent Areas. *Earth and Planetary Science Letters*, 442: 72–79. https://doi. org/10.1016/j. epsl.2016.03.003

Li, C., Yao, H. J., Yang, Y., et al., 2020. 3-D Shear Wave Velocity Structure in the Shallow Crust of the Tan-Lu Fault Zone in Lujiang, Anhui, and Adjacent Areas, and Its Tectonic Implications. *Earth and Planetary Physics*, 4(3): 317–328. https://doi.org/10.26464/epp2020026

Li, F., 2019. Physical Modelling of Xu-Huai Arc Structure on the Southeastern Margin of North China Block: [Dissertation]. Nanjing University, Nanjing (in Chinese with English Abstract)

Li, H. Y., Song, X. D., Lü, Q. T., et al., 2018. Seismic Imaging of Lithosphere Structure and Upper Mantle Deformation beneath East-Central China and Their Tectonic Implications. *Journal of Geophysical Research*: *Solid Earth*, 123(4): 2856–2870. https://doi.org/10.1002/2017jb014992

Li, L. L., Shen, W. S., Sui, S. Y., et al., 2021. Crustal Thickness beneath the Tanlu Fault Zone and Its Tectonic Significance Based on Two-Layer *H*-κ Stacking. *Earthquake Science*, 34(1): 47–63. https://doi.org/10.29382/eqs-2020-0064

Li, P. F., Sun, M., Rosenbaum, G., et al., 2017. Late Paleozoic Closure of the Ob-Zaisan Ocean along the Irtysh Shear Zone (NW China): Implications for Arc Amalgamation and Oroclinal Bending in the

Central Asian Orogenic Belt. *Geological Society of America Bulletin*, 129(5/6): 547–569. https://doi.org/10.1130/b31541.1

Li, W. C., 1994. The Genetics and Coal Resource Prospect of Xu-Huai Arc. *Coal Geology of China*, 8(2): 1–4 (in Chinese with English Abstract)

Ling, M. X., Li, Y., Ding, X., et al., 2013. Destruction of the North China Craton Induced by Ridge Subductions. *The Journal of Geology*, 121(2): 197–213. https://doi.org/10.1086/669248

Ling, M. X., Wang, F. Y., Ding, X., et al., 2009. Cretaceous Ridge Subduction along the Lower Yangtze River Belt, Eastern China. *Economic Geology*, 104(2): 303–321. https://doi.org/10.2113/gsecongeo.104.2.303

Liu, B. J., Feng, S. Y., Ji, J. F., et al., 2015. Fine Lithosphere Structure beneath the Middle-Southern Segment of the Tan-Lu Fault Zone. *Chinese Journal of Geophysics*, 58(5): 1610–1621 (in Chinese with English Abstract)

Liu, G., Gao, Y., Shi, Y. T., 2017. Shear-Wave Splitting in Qinling Orogen and Its Both Sides. *Chinese Journal of Geophysics*, 60(6): 2326–2337. https://doi.org/10.6038/cjg20170624 (in Chinese with English Abstract)

Liu, J., Wu, J. P., Wang, W. L., et al., 2020. Seismic Anisotropy beneath the Eastern Margin of the Tibetan Plateau from SKS Splitting Observations. *Tectonophysics*, 785: 228430. https://doi. org/10.1016/j.tecto.2020.228430

Livani, M., Scrocca, D., Arecco, P., et al., 2018. Structural and Stratigraphic Control on Salient and Recess Development along a Thrust Belt Front: The Northern Apennines (Po Plain, Italy). *Journal of Geophysical Research*: *Solid Earth*, 123(5): 4360 – 4387. https://doi. org/10.1002/2017jb015235

Lü, Q., Yan, J. Y., Shi, D. N., et al., 2013. Reflection Seismic Imaging of the Lujiang-Zongyang Volcanic Basin, Yangtze Metallogenic Belt: An Insight into the Crustal Structure and Geodynamics of an Ore District. *Tectonophysics*, 606: 60–77. https://doi.org/10.1016/j.tecto.2013.04.006

Luis, J. F., Miranda, J. M., 2008. Reevaluation of Magnetic Chrons in the North Atlantic between 35°N and 47°N: Implications for the Formation of the Azores Triple Junction and Associated Plateau. *Journal of Geophysical Research*: *Solid Earth*, 113(B10): B10105. https://doi.org/10.1029/2007jb005573

Luo, S., Huang, R., Zhu, L. P., et al., 2020. The Formation of the Dabashan Orocline, Central China: Insights from High-Resolution 3D Crustal Shear-Wave Velocity Structure. *Tectonophysics*, 774: 228244. https://doi.org/10.1016/j.tecto.2019.228244

Luo, S., Yao, H. J., Li, Q. S., et al., 2019. High-Resolution 3D Crustal S-Wave Velocity Structure of the Middle-Lower Yangtze River Metallogenic Belt and Implications for Its Deep Geodynamic Setting. *Science China Earth Sciences*, 62(9): 1361–1378. https://doi.org/10.1007/s11430-018-9352-9

Macedo, J., Marshak, S., 1999. Controls on the Geometry of Fold-Thrust Belt Salients. *Geological Society of America Bulletin*, 111(12): 1808–1822. https://doi.org/10.1130/0016-7606(1999)1111808: cotgof>2.3.co;2

Marshak, S., 1988. Kinematics of Orocline and Arc Formation in Thin-Skinned Orogens. *Tectonics*, 7(1): 73 – 86. https://doi. org/10.1029/tc007i001p00073

Marshak, S., 2004. Salients, Recesses, Arcs, Oroclines, and Syntaxes—A Review of Ideas Concerning the Formation of Map-View Curves in Fold-Thrust Belts. In: McClay, K. R., ed., Thrust Tectonics and Hydrocarbon Systems. *AAPG Memoir*, 82: 131–156

Meng, Q. R., Zhang, G. W., 1999. Timing of Collision of the North and South China Blocks: Controversy and Reconciliation. *Geology*, 27(2): 123–126. https://doi.org/10.1130/0091-7613(1999)0270123:tocotn>2.3.co;2

Meng, Y. F., Yao, H. J., Wang, X. Z., et al., 2019. Crustal Velocity Structure and Deformation Features in the Central-Southern Segment of Tanlu Fault Zone and Its Adjacent Area from Ambient Noise Tomography. *Chinese Journal of Geophysics*, 62(7): 2490 – 2509 (in Chinese with English Abstract)

Meurers, B., 2017. The Physical Meaning of Bouguer Anomalies—General Aspects Revisited. In: Pašteka, R., Mikuška, J., Meurers, B., eds., Understanding the Bouguer Anomaly (Chapter 2). Elsevier. 13–30

Mooney, W. D., Kaban, M. K., 2010. The North American Upper Mantle: Density, Composition, and Evolution. *Journal of Geophysical Research*: *Solid Earth*, 115(B12): B12424. https://doi.org/10.1029/2010jb000866

Pavlis, N. K., Holmes, S. A., Kenyon, S. C., et al., 2012. The Development and Evaluation of the Earth Gravitational Model 2008 (EGM2008). *Journal of Geophysical Research*: *Solid Earth*, 117(B4): B04406. https://doi.org/10.1029/2011jb008916

Ravat, D., 2007. Reduction to Pole. In: Gubbins, D., Herrero-Bervera, E., eds., Encyclopedia of Geomagnetism and Paleomagnetism. Springer, Dordrecht. 856–858

Schellart, W. P., Freeman, J., Stegman, D. R., et al., 2007. Evolution and Diversity of Subduction Zones Controlled by Slab Width. *Nature*, 446(7133): 308–311. https://doi.org/10.1038/nature05615

Shi, D. N., Lü, Q., Xu, W. Y., et al., 2013. Crustal Structure beneath the Middle-Lower Yangtze Metallogenic Belt in East China: Constraints from Passive Source Seismic Experiment on the Mesozoic Intra-Continental Mineralization. *Tectonophysics*, 606: 48–59. https://doi.org/10.1016/j.tecto.2013.01.012

Shi, W., Zhang, Y. Q., Dong, S. W., et al., 2012. Intra-Continental Dabashan Orocline, Southwestern Qinling, Central China. *Journal of Asian Earth Sciences*, 46: 20–38. https://doi.org/10.1016/j.jseaes.2011.10.005

Shu, L. S., Yin, H. W., Faure, M., et al., 2017. Mesozoic Intracontinental Underthrust in the SE Margin of the North China Block: Insights from the Xu-Huai Thrust-and-Fold Belt. *Journal of Asian Earth Sciences*, 141: 161–173. https://doi.org/10.1016/j.jseaes.2016.08.020

Sun, S. J., Yang, X. Y., Wang, G. J., et al., 2019. *In situ* Elemental and Sr-O Isotopic Studies on Apatite from the Xu-Huai Intrusion at the Southern Margin of the North China Craton: Implications for Petrogenesis and Metallogeny. *Chemical Geology*, 510: 200–214. https://doi.org/10.1016/j.chemgeo.2019.02.010

Sun, W. D., Ding, X., Hu, Y. H., et al., 2007. The Golden Transformation of the Cretaceous Plate Subduction in the West Pacific. *Earth and Planetary Science Letters*, 262(3/4): 533–542. https://doi.org/10.1016/j.epsl.2007.08.021

Sun, W. D., Ling, M. X., Yang, X. Y., et al., 2010. Ridge Subduction and Porphyry Copper-Gold Mineralization: An Overview. *Science China Earth Sciences*, 53(4): 475 – 484. https://doi. org/10.1007/s11430-010-0024-0

Tian, X. B., Santosh, M., 2015. Fossilized Lithospheric Deformation Revealed by Teleseismic Shear Wave Splitting in Eastern China. *GSA Today*, 25(2): 4–10. https://doi.org/10.1130/gsatg220a.1

Wang, G. L., Jiang, B., Cao, D. Y., et al., 1998. On the Xuzhou-Suzhou Arcuate Duplex-Imbricate. *Acta Geologica Sinica*, 72: 228–236 (in Chinese with English Abstract)

Wang, Q., Niu, F. L., Gao, Y., et al., 2016. Crustal Structure and Deformation beneath the NE Margin of the Tibetan Plateau Constrained by Teleseismic Receiver Function Data. *Geophysical Journal International*, 204(1): 167–179. https://doi.org/10.1093/gji/ggv420

Wang, R. R., Xu, Z. Q., Santosh, M., et al., 2019. Formation of Dabashan Arcuate Structures: Constraints from Mesozoic Basement Deformation in South Qinling Orogen, China. *Journal of Structural Geology*, 118:

135–149. https://doi.org/10.1016/j.jsg.2018.10.014

Weil, A. B., Sussman, A. J., 2004. Classifying Curved Orogens Based on Timing Relationships between Structural Development and Vertical-Axis Rotations. *Geological Society of America*, 383: 1–17. https://doi.org/10.1130/0-8137-2383-3(2004)383[1:ccobot]2.0.co;2

Wu, C. L., Xu, T., Badal, J., et al., 2015. Seismic Anisotropy across the Kunlun Fault and Their Implications for Northward Transforming Lithospheric Deformation in Northeastern Tibet. *Tectonophysics*, 659: 91–101. https://doi.org/10.1016/j.tecto.2015.07.030

Wüstefeld, A., Bokelmann, G., Barruol, G., 2010. Evidence for Ancient Lithospheric Deformation in the East European Craton Based on Mantle Seismic Anisotropy and Crustal Magnetics. *Tectonophysics*, 481(1/2/3/4): 16–28. https://doi.org/10.1016/j.tecto.2009.01.010

Xiong, S. Q., Yang, H., Ding, Y. Y., et al., 2016. Distribution of Igneous Rocks in China Revealed by Aeromagnetic Data. *Journal of Asian Earth Sciences*, 129: 231–242. https://doi.org/10.1016/j.jseaes.2016.08.016

Xu, J., Wang, K. D., Li, J. L., et al., 2021. High Resolution Tomography of the Tanlu Fault Zone near Hefei with Passive Seismic and Magnetotelluric Linear Array Data. *Earthquake Science*, 34(1): 24–35. https://doi.org.10.29382/eqs-2020-0061

Xu, S. T., Chen, G. B., Zhou, H. Y., 1987. Xuhuai Nappe. *Chinese Science Bulletin*, 32: 1091–1095 (in Chinese)

Xu, T., Zhang, Z. J., Tian, X. B., et al., 2014. Crustal Structure beneath the Middle-Lower Yangtze Metallogenic Belt and Its Surrounding Areas: Constraints from Active Source Seismic Experiment along the Lixin to Yixing Profile in East China. *Acta Petrologica Sinica*, 30(4): 918–930 (in Chinese with English Abstract)

Xu, W. L., Gao, S., Wang, Q. H., et al., 2006. Mesozoic Crustal Thickening of the Eastern North China Craton: Evidence from Eclogite Xenoliths and Petrologic Implications. *Geology*, 34(9): 721–724. https://doi.org/10.1130/g22551.1

Xu, X. M., Niu, F. L., Ding, Z. F., et al., 2018. Complicated Crustal Deformation beneath the NE Margin of the Tibetan Plateau and Its Adjacent Areas Revealed by Multi-Station Receiver-Function Gathering. *Earth and Planetary Science Letters*, 497: 204–216. https://doi.org/10.1016/j.epsl.2018.06.010

Yang, D. B., Xu, W. L., Pei, F. P., et al., 2008. Chronology and Pb Isotope Compositions of Early Cretaceous Adakitic Rocks in Xuzhou-Huaibei Area, Central China: Constraints on Magma Sources and Tectonic Evolution in the Eastern North China Craton. *Acta Petrologica Sinica*, 24(8): 1745–1758 (in Chinese with English Abstract)

Yang, X. Y., Li, H. Y., Li, Y. H., et al., 2019. Seismic Anisotropy beneath Eastern China from Shear Wave Splitting. *Geophysical Journal International*, 218(3): 1642–1651. https://doi.org/10.1093/gji/ggz242

Yin, A., 2010. Cenozoic Tectonic Evolution of Asia: A Preliminary Synthesis. *Tectonophysics*, 488(1/2/3/4): 293–325. https://doi. org/10.1016/j. tecto. 2009.06.002

Yin, A., Nie, S. Y., 1993. An Indentation Model for the North and South China Collision and the Development of the Tan-Lu and Honam Fault Systems, Eastern Asia. *Tectonics*, 12(4): 801–813. https://doi.org/10.1029/93tc00313

Yin, W. W., Lei, J. S., Du, M. F., et al., 2019. Uppermost-Mantle Pn Velocity and Anisotropic Tomography of the Tanlu Fault Zone and Adjacent Areas. *Chinese Journal of Geophysics*, 62(11): 4227–4238. https://doi.org//10.6038/cjg2019m0672 (in Chinese with English Abstract)

Yu, Y., Chen, Y. J., 2016. Seismic Anisotropy beneath the Southern Ordos Block and the Qinling-Dabie Orogen, China: Eastward Tibetan Asthenospheric Flow around the Southern Ordos. *Earth and Planetary Science Letters*, 455: 1–6. https://doi.org/10.1016/j.epsl.2016.08.026

Zeng, H. L., 2005. Gravity Field and Gravity Exploration. Geological Publishing House, Beijing. 79–100 (in Chinese)

Zhang, M. H., Xu, T., Lü, Q. T., et al., 2015. 3D Moho Depth beneath the Middle-Lower Yangtze Metallogenic Belt and Its Surrounding Areas: Insight from the Wide Angle Seismic Data. *Chinese Journal of Geophysics*, 58(12): 4360–4372. https://doi. org/10.6038/cjg20151203 (in Chinese with English Abstract)

Zhang, Y. Q., Dong, S. W., 2008. Mesozoic Tectonic Evolution History of the Tan-Lu Fault Zone, China: Advances and New Understanding. *Geological Bulletin of China*, 27: 1371–1390 (in Chinese with English Abstract)

Zhang, Y. Q., Vergèly, P., Mercier, J. L., et al., 1999. Kinematic History and Changes in the Tectonic Stress Regime during the Cenozoic along the Qinling and Southern Tanlu Fault Zones. *Acta Geologica Sinica—English Edition*, 73(3): 264–274. https://doi. org/10.1111/j. 1755-6724.1999.tb00835.x

Zhang, Z. K., Ling, M. X., Lin, W., et al., 2020. "Yanshanian Movement" Induced by the Westward Subduction of the Paleo-Pacific Plate. *Solid Earth Sciences*, 5(2): 103–114. https://doi. org/10.1016/j. sesci.2020.04.002

Zhao, L., Zheng, T. Y., Lu, G., 2013. Distinct Upper Mantle Deformation of Cratons in Response to Subduction: Constraints from SKS Wave Splitting Measurements in Eastern China. *Gondwana Research*, 23(1): 39–53. https://doi.org/10.1016/j.gr.2012.04.007

Zhao, T., Zhu, G., Lin, S. Z., et al., 2016. Indentation-Induced Tearing of a Subducting Continent: Evidence from the Tan-Lu Fault Zone, East China. *Earth-Science Reviews*, 152: 14–36. https://doi. org/10.1016/j.earscirev.2015.11.003

Zheng, Y. F., 2008. A Perspective View on Ultrahigh-Pressure Metamorphism and Continental Collision in the Dabie-Sulu Orogenic Belt. *Chinese Science Bulletin*, 53(20): 3081–3104. https://doi. org/10.1007/s11434-008-0388-0

Zhu, G., Wang, D. X., Liu, G. S., et al., 2004. Evolution of the Tan-Lu Fault Zone and Its Responses to Plate Movement in West Pacific Basin. *Chinese Journal of Geology*, 39(1): 36–49 (in Chinese with English Abstract)

Zhu, G., Liu, G. S., Niu, M. L., et al., 2009. Syn-Collisional Transform Faulting of the Tan-Lu Fault Zone, East China. *International Journal of Earth Sciences*, 98(1): 135–155. https://doi.org/10.1007/s00531-007-0225-8

Zhu, L. P., Kanamori, H., 2000. Moho Depth Variation in Southern California from Teleseismic Receiver Functions. *Journal of Geophysical Research*: *Solid Earth*, 105(B2): 2969–2980. https://doi.org/10.1029/1999jb900322